Trisaccharide containing α2,3-linked sialic acid is a receptor for mumps virus

Marie Kubota[a], Kaoru Takeuchi[b,1], Shumpei Watanabe[a], Shinji Ohno[a], Rei Matsuoka[c], Daisuke Kohda[c], Shin-ichi Nakakita[d], Hiroaki Hiramatsu[e], Yasuo Suzuki[e], Tetsuo Nakayama[f], Tohru Terada[g], Kentaro Shimizu[g], Nobutaka Shimizu[h], Mitsunori Shiroishi[i], Yusuke Yanagi[a], and Takao Hashiguchi[a,1]

[a]Department of Virology, Faculty of Medicine, Kyushu University, Fukuoka 812-8582, Japan; [b]Laboratory of Environmental Microbiology, Faculty of Medicine, University of Tsukuba, Tsukuba 305-8575, Japan; [c]Division of Structural Biology, Medical Institute of Bioregulation, Kyushu University, Fukuoka 812-8582, Japan; [d]Department of Functional Glycomics, Life Science Research Center, Kagawa University, Kagawa 761-0793, Japan; [e]Health Science Hills, College of Life and Health Sciences, Chubu University, Kasugai 487-8501, Japan; [f]Laboratory of Viral Infection, Kitasato Institute for Life Sciences, Tokyo 108-8641, Japan; [g]Department of Biotechnology and Agricultural Bioinformatics Research Unit, Graduate School of Agricultural and Life Sciences, The University of Tokyo, Tokyo 113-8657, Japan; [h]Photon Factory, Institute of Materials Structure Science, High-Energy Accelerator Research Organization, Tsukuba 305-0801, Japan; and [i]Graduate School of Pharmaceutical Sciences, Kyushu University, Fukuoka 812-8582, Japan

Edited by Michael B. A. Oldstone, The Scripps Research Institute, La Jolla, CA, and approved August 19, 2016 (received for review May 25, 2016)

Mumps virus (MuV) remains an important pathogen worldwide, causing epidemic parotitis, orchitis, meningitis, and encephalitis. Here we show that MuV preferentially uses a trisaccharide containing α2,3-linked sialic acid in unbranched sugar chains as a receptor. Crystal structures of the MuV attachment protein hemagglutinin-neuraminidase (MuV-HN) alone and in complex with the α2,3-sialylated trisaccharide revealed that in addition to the interaction between the MuV-HN active site residues and sialic acid, other residues, including an aromatic residue, stabilize the third sugar of the trisaccharide. The importance of the aromatic residue and the third sugar in the MuV-HN–receptor interaction was confirmed by computational energy calculations, isothermal titration calorimetry studies, and glycan-binding assays. Furthermore, MuV-HN was found to bind more efficiently to unbranched α2,3-sialylated sugar chains compared with branched ones. Importantly, the strategically located aromatic residue is conserved among the HN proteins of sialic acid-using paramyxoviruses, and alanine substitution compromised their ability to support cell–cell fusion. These results suggest that not only the terminal sialic acid but also the adjacent sugar moiety contribute to receptor function for mumps and these paramyxoviruses. The distribution of structurally different sialylated glycans in tissues and organs may explain in part MuV's distinct tropism to glandular tissues and the central nervous system. In the crystal structure, the epitopes for neutralizing antibodies are located around the α-helices of MuV-HN that are not well conserved in amino acid sequences among different genotypes of MuV. This may explain the fact that MuV reinfection sometimes occurs.

structure | entry | receptor | infection | paramyxovirus

Mumps virus (MuV), an important aerosol-transmitted human pathogen, affects the parotid and other salivary glands, pancreas, testis, ovary, mammary glands, and kidney (1). It also infects the central nervous system, causing meningitis and, less frequently, encephalitis and unilateral nerve deafness. The hallmarks of MuV infection were described in the fifth century BC by Hippocrates (1). To prevent this disease, inactivated and live attenuated MuV vaccines were developed in 1946 and 1958, respectively (1). Currently, MuV vaccine is usually given as a live measles–mumps–rubella (MMR) vaccine. Although the cellular receptors and structures of viral glycoproteins, the main target of neutralizing antibodies (Abs), have been well characterized for measles and rubella viruses (2–4), the exact identity of a receptor for MuV and the crystal structure of its attachment glycoprotein remain to be determined. Although the MMR vaccine has dramatically reduced the prevalence of MuV infection (1), MuV vaccine-induced meningitis, a main adverse reaction, occurs at a rate ranging from 1/400 to 1/1,000,000 of vaccinated individuals, depending on the strain (1). Other studies have reported infection, as well as reinfection, among highly vaccinated populations (5, 6).

MuV is classified into 12 genotypes, which are used for surveillance by the World Health Organization (1). The vaccine strains currently used worldwide belong to genotype A, B, H, or N (1). Although MuV is thought to be serologically monotypic (1, 7), some studies have reported that MuV genotype-specific Abs are produced (8, 9). Thus, the antigenic variation among different genotypes is a concern for MuV vaccination and natural infection (5, 7).

MuV is a member of the genus *Rubulavirus* in the family *Paramyxoviridae*. Paramyxoviruses, enveloped and nonsegmented negative-strand RNA viruses, enter the host cell by attaching to a cell surface receptor via hemagglutinin-neuraminidase (HN), hemagglutinin (H), or glycoprotein (G), depending on the virus, and cause membrane fusion through the action of the fusion (F) protein (10). The attachment proteins (HN, H, and G) are the major targets of neutralizing Abs, along with the F protein (1). The MuV genome contains 15,384 nucleotides encoding nucleocapsid, phospho, matrix, F, small hydrophobic, HN, and large proteins (1). Sialic acid, expressed on the cell surface as a nonreducing terminal component of sugar chains, is believed to be the common receptor for many paramyxoviruses including MuV, and influenza viruses (10, 11). Human and avian influenza viruses

Significance

Despite the availability of an effective vaccine, mumps virus (MuV) still causes outbreaks even in highly vaccinated populations worldwide. MuV affects the salivary glands, testicles, ovaries, pancreas, meninges, and brain. This characteristic tropism to glandular tissues and the central nervous system remains to be explained. Here, using X-ray crystallography, computational energy calculations, isothermal titration calorimetry, glycan-binding assays, and MuV glycoprotein-mediated cell fusion assays, we show that the trisaccharide containing an α2,3-linked sialic acid on the cell surface acts as a receptor for MuV. In conjunction with elucidation of the distribution of structurally different sialylated glycans in tissues and organs, this finding will lead to a better understanding of MuV tropism and pathogenesis.

Author contributions: M.K., K.T., Y.Y., and T.H. designed research; M.K., K.T., S.W., S.O., R.M., S.-i.N., H.H., T.N., T.T., N.S., M.S., and T.H. performed research; M.K., K.T., R.M., D.K., S.-i.N., H.H., Y.S., T.N., T.T., K.S., N.S., M.S., Y.Y., and T.H. analyzed data; and M.K., Y.Y., and T.H. wrote the paper.

The authors declare no conflict of interest.

This article is a PNAS Direct Submission.

Data deposition: The atomic coordinates and structure factors have been deposited in the Protein Data Bank, www.wwpdb.org [PDB ID codes 5B2C (MuV-HN) and 5B2D (MuV-HN−3′-SL)].

[1]To whom correspondence may be addressed. Email: ktakeuch@md.tsukuba.ac.jp or takaoh@virology.med.kyushu-u.ac.jp.

This article contains supporting information online at www.pnas.org/lookup/suppl/doi:10.1073/pnas.1608383113/-/DCSupplemental.

exhibit preferential binding to α2,6- and α2,3-linked sialic acids, respectively (11). The distinct preference for either of the two major types of sialic acid is an important determinant of the influenza virus host range (11). Whether MuV uses a particular sialylated sugar structure as a receptor is unknown.

In this study, we first determined the crystal structures of the MuV-HN protein (hereinafter abbreviated as MuV-HN) receptor-binding head domain alone and in complex with trisaccharides containing sialic acid. Based on the structures thus obtained, we further examined the MuV-HN–receptor interaction using computational calculations, isothermal titration calorimetry (ITC) studies, glycan-binding assays, and functional studies. The structures of MuV-HN also provided important insights into the mechanism of Ab-mediated neutralization.

Results

Overall Structures of the MuV-HN Head Domain Alone and in Complex with Sialyllactose. MuV-HN comprises an N-terminal cytoplasmic tail, transmembrane region, stalk, and C-terminal receptor-binding head domain (1). To gain insight into the MuV–receptor interaction, we determined the crystal structure of MuV-HN. The HN head domain of the MuV Hoshino strain was expressed in HEK293S cells lacking *N*-acetylglucosaminyltransferase I [293S GnTI(−) cells], which allows glycoproteins to possess homogeneously modified glycans and thus aids in the production of better-diffracting crystals (12). The purified MuV-HN head domain was methylated following a previously developed method (13) and crystallized. Diffraction to 2.24-Å resolution was obtained for a single crystal of the MuV-HN head domain. Its structure was determined by molecular replacement using Newcastle disease virus-HN (14) as a search model and was refined to an R_{work} value of 20.2% and an R_{free} value of 22.2% (Table S1). In addition, the MuV-HN head domain was cocrystallized with two types of sialyllactose, 3′-sialyllactose (3′-SL) and 6′-sialyllactose (6′-SL), as the sialic acid-containing receptor analogs. These are trisaccharides in which the terminal *N*-acetylneuraminic acid (hereinafter referred to as Sia-1) is connected to the galactosyl unit (referred to as Gal-2) of lactose by the α2,3-linkage and the α2,6-linkage, respectively. (The glucose unit of lactose is referred to as Glc-3.) The cocrystal structure with 3′-SL was determined at 2.18-Å resolution and was refined to an R_{work} value of 17.6% and an R_{free} value of 19.1% (Table S1). Two monomers are contained in the asymmetric unit of both free and 3′-SL–bound forms of the MuV-HN head domain.

The MuV-HN head domain exhibits a six-bladed β-propeller fold (β1–β6 sheets) and forms a homodimer (Fig. 1 *A* and *B*). The two monomers forming a dimer are tilted approximately 90° to each other. Similar to attachment proteins of other paramyxoviruses (14–17), two dimers form a tetramer (dimer of dimers) (Fig. S1*A*). The ligand 3′-SL is bound to the top pocket of the MuV-HN head domain (Fig. 1*B* and Fig. S1*A*). In the homodimer, no large structural difference is observed between the free and receptor-bound forms of the MuV-HN head domain (rmsd of 0.40 Å; 882 Cα atoms in the dimer) (Fig. S1*B*).

The structure of the MuV-HN head domain cocrystallized with 6′-SL was also determined. However, the electron density for 6′-SL was not detected in the structure, suggesting that MuV-HN does not efficiently bind 6′-SL.

Interaction of MuV-HN and 3′-SL. In the crystal structure of MuV-HN complexed with 3′-SL, the aromatic residues Tyr268 and Phe370 are stacked together with Tyr369, which interacts face to face with Glc-3 of 3′-SL. The O^{η} oxygen atom of Tyr369 hydrogen bonds with the O1 oxygen atom of Glc-3 and the O1 oxygen atom of Gal-2 (Fig. 1*C*, *Left*). Furthermore, Val476 stabilizes Glc-3 by hydrogen bonding through its main chain with the O6 oxygen atom of the sugar, and by forming a hydrophobic interaction with Glc-3 through its side chain. Notably, Tyr369, and Val476 are conserved among all genotypes of MuV, but they are not among the seven active site residues highly conserved in viral and cellular sialidases, which are responsible for sialic acid recognition (18). The active site residues correspond to Arg180, Glu407, Arg422, Arg512, Tyr540, Glu561, and Asp204 in the HN proteins of MuV, and these seven residues are, as expected, conserved among all genotypes of MuV. The first five of these residues are involved in the direct binding to Sia-1 of 3′-SL, and

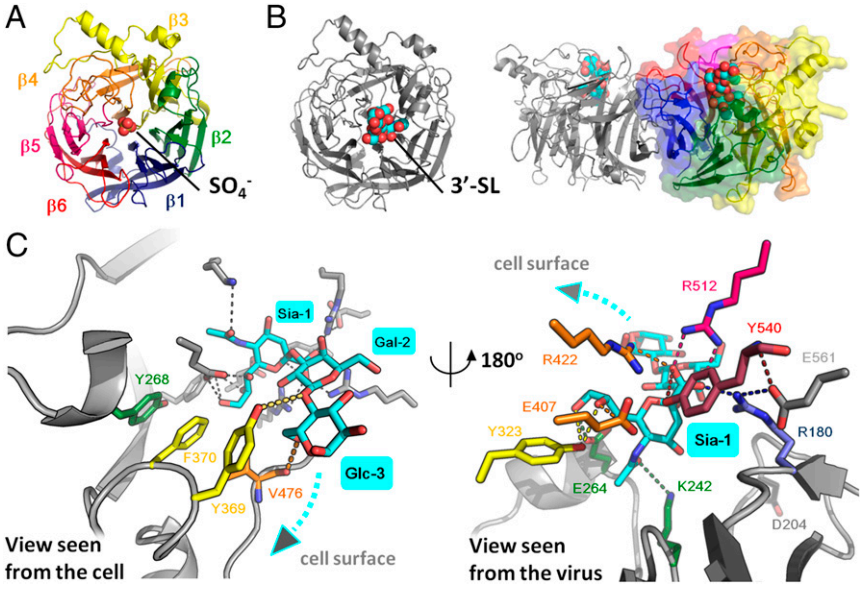

Fig. 1. Structures of the MuV-HN head domain. (*A*) Top view of the MuV-HN monomer in the absence of receptor whose β-sheets (β1–β6) are rainbow in color. The SO_4^- ion is shown in spheres. (*B*) MuV-HN monomer (*Left*, top view) and homodimer (*Right*, side view) bound to 3′-SL. 3′-SL is shown in spheres. (*C*) MuV-HN residues involved in receptor binding. The MuV-HN residues involved in the interaction with Glc-3 and Gal-2 of 3′-SL (cyan) (*Left*, view seen from the cell) and with Sia-1 of 3′-SL (*Right*, view seen from the virus) are indicated by the same rainbow colors as in *A*. The other active site residues, E561 and D204, conserved among paramyxoviruses, are colored in gray. Nitrogen atom, blue; oxygen atom, red.

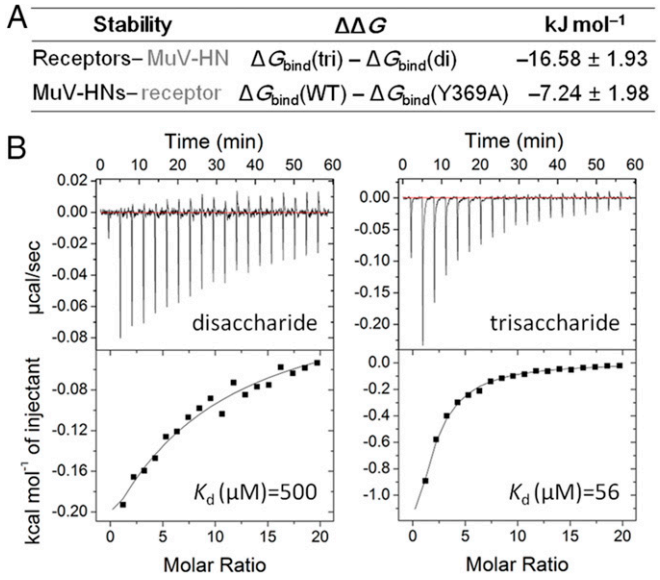

Fig. 2. Stability of the MuV HN protein-receptor complex. (*A*) The energetic stability of the HN protein–receptor interaction calculated with the MD simulations. di, disaccharide; tri, trisaccharide. (*B*) ITC analysis of the binding of glycans to the MuV-HN protein. (*Upper*) Raw titration data. (*Lower*) Integration plot of the titration data. (*Left*) MuV-HN protein–NeuAcα2,3Gal (disaccharide). (*Right*) MuV-HN protein–NeuAcα2,3Galβ1,4Glc (trisaccharide).

Lys242, Glu264, and Tyr323 also bind to Sia-1, along with the five residues (Fig. 1*C*, *Right*). Glu561 appears to support the conformations of the side chain of Arg180 and the main chain of Tyr540, but does not appear to be involved in direct binding to Sia-1. Another active site residue, Asp204, points away from Sia-1 and does not contribute to HN's interaction with it (Fig. 1*C*, *Right*). In the absence of 3′-SL, an SO_4^- ion is observed within the top pocket of the MuV-HN head domain under the crystallization condition in which the crystallization buffer contains sulfate (Fig. 1*A*). In MuV-HN cocrystallized with 3′-SL, the ion's density disappears and is replaced by 3′-SL (Fig. 1*B*). In the human body, a PO_4^- ion instead of an SO_4^- ion may be present at that position, so that the HN protein is stabilized before it binds to a receptor.

The foregoing observations suggested to us that the saccharide moiety underlying the terminal sialic acid also plays an important role in the MuV HN–receptor interaction.

Stability of the HN Protein–Receptor Interaction. In an attempt to evaluate the energetic stability of the MuV-HN protein-receptor complex, we first compared sialic acid-containing trisaccharides and disaccharides for their ability to interact with MuV-HN based on molecular dynamics (MD) simulations. Computational calculations revealed that the trisaccharide 3′-SL exhibits more stable binding to MuV-HN ($\Delta\Delta G = -16.58 \pm 1.93$ kJ/mol) than the disaccharide Sia-1–Gal-2 (Fig. 2*A* and Fig. S2*A*). We also compared energetic stability in the wild type (WT) of MuV-HN and its mutant in which Tyr-369 was replaced with Ala (Y369A). Our calculations showed that the WT binds more stably to 3′-SL ($\Delta\Delta G = -7.24 \pm 1.98$ kJ/mol) compared with the mutant (Fig. 2*A* and Fig. S2*B*). These results support the idea that the third sugar of 3′-SL and Tyr369 of MuV-HN contribute substantially to the MuV HN–receptor interaction.

We also examined the binding affinity of the MuV-HN protein receptor using ITC studies. Consistent with the computational calculations, the trisaccharide 3′-SL exhibited much stronger binding affinity to the MuV-HN protein ($K_d = 56$ μM) compared with the disaccharide Sia-1–Gal-2 ($K_d = 500$ μM) (Fig. 2*B*).

MuV-HN Preferentially Binds to Oligosaccharides Containing α2,3-Linked Sialic Acid. We next examined the binding of MuV-HN to six types of glycans containing α2,3- or α2,6-linked sialic acid (G1–G6 in Fig. 3*A*) using a glycoconjugate-spotted microplate (19, 20). The glycoconjugates represent major sialylated glycans found in the human respiratory tract (21), and their structural compositions are described in Fig. 3*A*. Fluorescence due to the binding of MuV-HN was observed for G1 and less strongly for G2 (Fig. 3*A*). G1 and G2 are glycans containing α2,3-linked sialic acid. Only a limited amount of fluorescence was observed for G3 and glycans containing α2,6-linked sialic acid, including G4, G5, and G6. On a different plate containing sialylated and non-sialylated glycans (22), MuV-HN was found to exhibit binding to NeuAcα2,3Galβ1,4Glc-BSA and NeuAcα2,3Galβ1,4GlcNAc-polyglutamine, but only low levels of binding to the other glycans examined (Fig. S3). We also tested the binding of the MuV-HN Y369A mutant to NeuAcα2,3Galβ1,4GlcNAc-polyglutamine and NeuAcα2,3Galβ1,4Glc-BSA (Fig. 3*B*). The mutant exhibited a

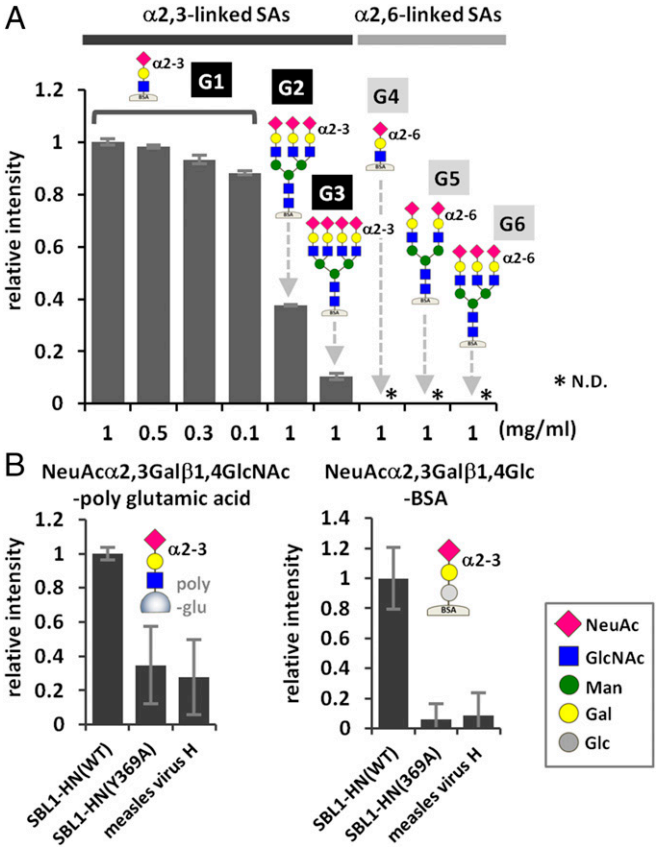

Fig. 3. Binding of MuV-HN proteins to sialyl glycans. (*A*) Binding of purified MuV-HN protein to six branched/unbranched α2,3- or α2,6-linked sialyl glycans. G1, NeuAcα2,3Galβ1,4GlcNAc-BSA; G2, NeuAcα2,3Galβ1,4GlcNAc β1,2(NeuAcα2,3Galβ1,4GlcNAcβ1,4)Manα1,3(NeuAcα2,3Galβ1,4GlcNAcβ1,2Manα1,6)Manβ1,4GlcNAcβ1,4GlcNAc-BSA; G3, NeuAcα2,3Galβ1,4GlcNAcβ1,2(NeuAcα2,3Galβ1,4GlcNAcβ1,4)Manα1,3(NeuAcα2,3Galβ1,4GlcNAcβ1,2 (NeuAcα2,3Galβ1,4GlcNAcβ1,6)Manα1,6)Manβ1,4GlcNAcβ1,4GlcNAc-BSA; G4, NeuAcα2,6Galβ1,4GlcNAc-BSA; G5, NeuAcα2,6Galβ1,4GlcNAcβ1,2Manα1,3(NeuAcα2,6Galβ1,4GlcNAcβ1,2Manα1,6)Manβ1,4GlcNAcβ1,4GlcNAc-BSA; G6, NeuAcα2,6Galβ1,4GlcNAcβ1,2(NeuAcα2,6Galβ1,4GlcNAcβ1,4)Manα1,3 (NeuAcα2,6Galβ1,4GlcNAcβ1,2Manα1,6)Manβ1,4GlcNAcβ1,4GlcNAc-BSA. The glycans are attached onto BSA. (*B*) Binding of purified MuV-HN proteins, WT or Y369A, to the trisaccharides NeuAcα2,3Galβ1,4GlcNAc-polyglutamic acid (*Left*) and NeuAcα2,3Galβ1,4Glc-BSA (*Right*). Measles virus H protein served as a negative control. Data are the mean ± SD of three samples. N.D., not detected. Data shown in this figure are representative of three independently performed experiments.

decreased level of binding to both glycans containing α2,3-linked sialic acid compared with the WT.

In the foregoing studies, the HN protein (amino acid positions 96–582) of the MuV SBL-1 strain (genotype A) was used. We also examined the binding of mumps virions of the SBL-1, Tokyo M-21 (genotype G), and Tokyo S-III-10 (genotype L) strains (23), as well as the purified HN protein of the MuV Hoshino strain (genotype B), to α2,3- and α2,6-linked sialyl glycopolymers (Neu5Acα2,3Galβ1,4GlcNAcβ-pAP and Neu5Acα2,6Galβ1,4GlcNAcβ-pAP) (24) on microplates. All MuV particles examined bound to α2,3-linked sialyl glycopolymers, but not to α2,6-linked sialyl glycopolymers (Fig. S4).

These binding assays indicate that MuV-HN preferentially binds to oligosaccharides containing α2,3-linked sialic acid, and that branching of saccharides tends to decrease the binding. The results also reveal that Tyr369 in MuV-HN, which interacts with the third sugar (Glc-3) of 3′-SL (Fig. 1*C*, *Left*), is critical for the binding of MuV HN to oligosaccharides containing α2,3-linked sialic acid.

α2,3-Linked Sialic Acid Is Necessary for MuV-Mediated Cell–Cell Fusion and Entry. To evaluate the importance of α2,3-linked sialic acid in MuV receptor function, we cleaved α2,3-linked sialic acid from the cell surface using sialidases. The amounts of α2,3- and α2,6-linked sialic acids on HEK293 cells, as evaluated by flow cytometry, were close to the background levels after treatment with *Arthrobacter ureafaciens* sialidase, which cleaves both the α2,3 and α2,6 linkages of *N*-acetylneuraminic acid (Fig. S5*A*). The α2,3- and α2,6-linked sialic acids were detected by binding to the *Maackia amurensis* lectin II (MAL II) and *Sambucus nigra* agglutinin (SNA), respectively. Treatment with *Salmonella typhimurium* α2,3-sialidase also resulted in lower levels of α2,3-linked sialic acid on the cell surface, although the reduction was not as complete as that seen with *A. ureafaciens* sialidase. As expected, the amount of α2,6-linked sialic acid on the cell surface was not affected by treatment with α2,3-sialidase.

We next performed a fusion assay to assess the effect of sialic acid cleavage on cell–cell fusion mediated by MuV HN and F proteins. HEK293 cells were transiently transfected with the expression plasmid encoding EGFP. These HEK293-EGFP cells were then treated with α2,3-sialidase, *A. ureafaciens* sialidase, or control medium. HEK293 cells in different dishes were transfected with the expression plasmids encoding HN and F proteins of MuV. After 20 h of sialidase treatment, HEK293-EGFP cells were overlaid onto HEK293 cells expressing MuV HN and F proteins (Fig. S5*B*). If HEK293-EGFP cells (treated or untreated with sialidases) fuse with HEK293 cells expressing the HN and F proteins, then EGFP-positive syncytia will be observed. EGFP-positive syncytia were clearly detected at 15 min after the overlay in the control cell mixture containing sialidase-untreated HEK293-EGFP cells, but not in the cell mixture containing α2,3-sialidase–treated or *A. ureafaciens* sialidase-treated HEK293-EGFP cells (Fig. 4*A*). The size and number of EGFP-expressing syncytia increased gradually with time (at 30 and 60 min) in the control cell mixture. In contrast, the cell mixture containing α2,3-sialidase–treated or *A. ureafaciens* sialidase-treated HEK293-EGFP cells formed a reduced number of small EGFP-expressing syncytia at 30 min or 60 min after overlay, respectively. Residual and/or regenerated (or recycled) α2,3-linked sialic acid on sialidase-treated HEK293-EGFP cells presumably supported syncytium formation in these cell mixtures at later time points. The same results were obtained with the respiratory epithelial cell line NCI-H358 or the neuroblastoma cell line IMR-32 when these cells instead of HEK293 cells were transfected with EGFP, treated with sialidases and overlaid onto HEK293 expressing MuV HN and F proteins (Fig. S5 *A*, *C*, and *D*). Sialidase treatment had no affect on the cell–cell fusion mediated by the H and F proteins of the measles virus, owing to the proteinaceous nature of the receptors (Fig. S5*E*).

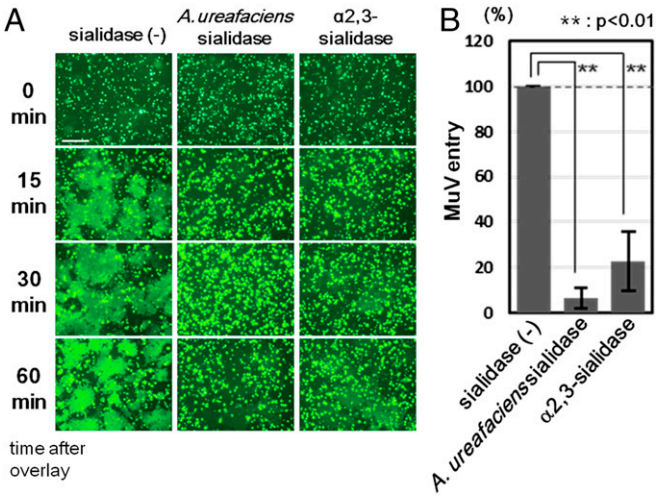

Fig. 4. Effect of cleavage of sialic acid on MuV-induced cell–cell fusion and MuV entry. (*A*) HEK293 cells expressing EGFP were treated with control medium, α2,3-sialidase, or *A. ureafaciens* sialidase. They were detached from the plates and then overlaid onto HEK293 cells expressing the HN and F proteins of MuV. The cells were observed under fluorescence microscopy at 0, 15, 30, and 60 min after overlay. (Scale bar: 200 μm.) (*B*) HEK293 cells pretreated with control medium, α2,3-sialidase, or *A. ureafaciens* sialidase were infected with the EGFP-expressing recombinant MuV. At 24 h post-infection, EGFP-positive cells were counted to evaluate the efficiency of virus entry. The control was set to 100, and data indicate the mean ± SD of triplicate experiments. The data are representative of three independently performed experiments. $^{**}P < 0.01$, two-tailed Student's *t* test.

We also examined MuV entry into sialidase-treated cells. HEK293 cells that had been treated with α2,3-sialidase, *A. ureafaciens* sialidase, or control medium were infected with EGFP-expressing recombinant MuV. Entry efficiencies in α2,3-sialidase–treated and *A. ureafaciens* sialidase-treated HEK293 cells were 20% and ∼8%, respectively, of that seen in control cells (Fig. 4*B*).

Interaction of the HN Protein with the Third Sugar from the Nonreducing Terminal of Saccharide Also Contributes to Paramyxovirus-Mediated Cell–Cell Fusion. Given that our structural and binding studies indicated the involvement of Glc-3 at the base of the terminal sialic acid in the interaction with MuV-HN, we examined the functional role of this third sugar of the trisaccharide. HEK293 cells were transfected with the expression plasmid encoding the HN protein of the MuV Hoshino strain or its mutant with the Y369A substitution (Fig. 5*A*, *Left*), together with the expression plasmids encoding the MuV F protein and EGFP, respectively. The mutant HN protein was expressed on the cell surface as efficiently as the WT protein, as assessed by flow cytometry (Fig. S6*A*). The cells transfected with the mutant HN protein apparently produced a lower level of cell–cell fusion compared with cells transfected with the WT HN protein (Fig. 5*A*, *Right*). The same results were obtained with NCI-H358 and IMR-32 cells (Fig. S6*B*).

To test whether this finding would also hold true for other paramyxoviruses using sialic acid as a receptor, we examined HN proteins of parainfluenza virus 5 (PIV5), human parainfluenza virus 2 (PIV2), and Sendai virus (SeV). PIV5 and PIV2, like MuV, belong to the genus *Rubulavirus*, whereas SeV is a member of the genus *Respirovirus*. The structures of the PIV5 HN protein unbound and bound to the receptor have been determined (16), but those of the PIV2 and SeV HN proteins have not; therefore, we generated the model structures for the HN proteins of the latter two viruses based on the known HN structures of other

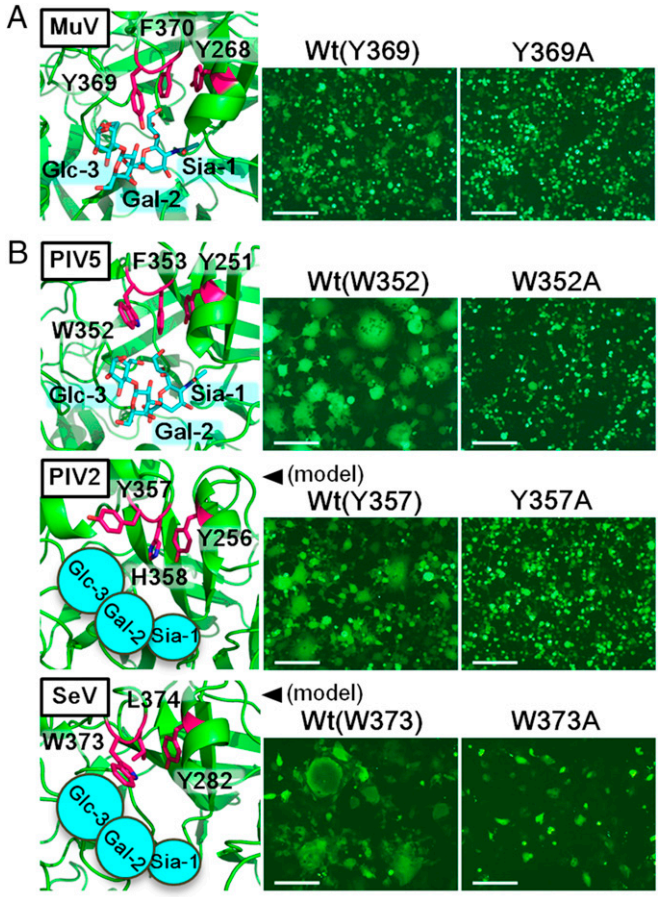

Fig. 5. Involvement of the third sugar from the nonreducing terminal in the HN protein–receptor interaction. Experiments were performed for the HN protein of MuV (*A*) and PIV5, PIV2, and SeV (*B*). (*Left*) Aromatic residues involved in the interaction with the third sugar from the nonreducing terminal (Glc-3 of SL) as well as residues stacked with them in solved (MuV and PIV5) or model HN protein structures (PIV2 and SeV) are shown in magenta. SLs (Sia-1, Gal-2, and Glc-3) are shown in cyan. (*Right*) HEK293 (MuV, PIV5, and PIV2) or Vero (SeV) cells transfected with expression plasmids encoding the HN protein (WT or mutant), F protein, and EGFP were observed for syncytia formation using fluorescence microscopy at 2 d posttransfection. (Scale bar: 200 μm.)

paramyxoviruses, including PIV5 and PIV3 (16, 17). These solved and model structures show that Trp352, Tyr357, and Trp373 of PIV5, PIV2, and SeV HN proteins, respectively, interact with Glc-3 of sialyllactose (Fig. 5*B*, *Left*), similar to Tyr369 of MuV-HN. We mutated these residues to alanine and then tested the ability of the mutant HN proteins to support cell–cell fusion in conjunction with the corresponding F proteins. All of the mutant HN proteins were expressed on the cell surface as efficiently as the WT proteins (Fig. S6*A*), but induced cell fusion much less efficiently (Fig. 5*B*). These results indicate that in addition to the terminal sialic acid, the third sugar from the nonreducing terminal contributes to the HN protein–receptor interaction. (The structures suggest that the fourth sugar, rather than the third sugar, from the nonreducing terminal may interact with the aromatic residues of PIV5 and PIV2.)

Discussion

It is generally believed that the sialic acid on glycans is a receptor for paramyxoviruses belonging to the genera *Respirovirus*, *Rubulavirus*, and *Avulavirus* (10), but whether structures other than the terminal sialic acid are directly involved in the interaction with the HN proteins of these paramyxoviruses is unknown. Our findings indicate that the third sugar from the nonreducing terminal of glycans also contributes to the receptor–HN protein interaction in MuV, and that a trisaccharide containing α2,3-linked sialic acid is the core structure of a receptor for MuV.

In the X-ray crystal structures, the electron density of the trisaccharide was detected in the MuV-HN head domain cocrystalized with 3′-SL, but not in that cocrystallized with 6′-SL. Importantly, the crystal structures revealed that the binding of 3′-SL to MuV-HN not only is mediated by the MuV-HN–sialic acid interaction, but also is stabilized by the interaction between Gal-2/Glc-3 of 3′-SL and Tyr369/Val476 of MuV-HN. The stacking interaction of Tyr369 with the adjacently located Phe370 and Tyr268 also may contribute to the stability of the interaction with Glc-3. The Y369A substitution considerably reduced cell–cell fusion mediated by the HN and F proteins. Because the Y369A substitution is unlikely to dramatically affect the conformation of the MuV-HN monomer, the conformation of the dimer, or the orientation of the tetramer, the lack of interaction between MuV-HN and Glc-3 must be the reason for the reduced cell–cell fusion. Computational calculations using the MD simulations and binding-affinity evaluation by ITC also support the importance of both the aromatic residue at this position of MuV-HN and the third sugar from the nonreducing terminal of the trisaccharide for the stability of the MuV-HN–sugar complex. The importance of the third sugar–HN aromatic residue interaction also appears to apply to the paramyxoviruses PIV5, PIV2, and SeV. Thus, we may have to reconsider the structural properties of receptors for other sialic acid-using viruses as well.

The finding that MuV-HN favors α2,3-linked sialic acid over α2,6-linked sialic acid was supported by the results of glycan binding assays and cell–cell fusion studies after sialidase treatment. The 3′-SL (used for crystal studies and the glycan-binding assay) may constitute the terminal structure of glycosphingolipids, whereas 3′-sialyllactosamine (used for the glycan binding assay) exists as the terminal sugar of *N*-linked and *O*-linked glycoproteins (25). The sole difference between these trisaccharides is the acetylation of Glc-3 in the latter. The binding of MuV-HN to both types of sugars suggests that MuV could use glycosphingolipids and/or glycoproteins as receptors (Fig. 3*B* and Fig. S4). The crystal structure of MuV-HN bound to 3′-SL also suggests that the acetylation of Glc-3 does not spatially inhibit the interaction of the trisaccharide containing α2,3-linked sialic acid with Tyr369 and other residues of MuV-HN. Because the MuV-HN residues involved in the interaction with 3′-SL are highly conserved, the trisaccharide containing the α2,3-linked sialic acid is likely essential for all genotypes of MuV. In fact, MuV strains of the genotypes A, B, G, and L all exhibited a preference for glycans containing α2,3-linked sialic acid, although genotype A has different antigenicity than the others (23).

Interestingly, MuV-HN bound more strongly to the simple α2,3-sialylated trisaccharide than to the branched α2,3-sialylated oligosaccharides, and its binding was weaker to a tetra-antennary complex glycan than to a triantennary complex glycan. The results suggest that additional sugars at the base of the sialylated trisaccharide may affect the interaction with MuV-HN via steric hindrance. Sialylated glycans have highly diverse structures and compositions (25). It has been shown that α2,6- and α2,3-linked sialic acids are largely present in the upper and lower respiratory tracts in humans, respectively (11); however, the systemic distribution of structurally different glycans in tissues and organs remains to be adequately characterized. A more detailed study may shed light on MuV's distinct tropism to glandular tissues and the central nervous system.

The crystal structure of MuV-HN also provides insight into the mechanism by which Abs induced by natural infection and vaccination neutralize MuV. When mapped on the structure of

MuV-HN, the great majority of the reported epitopes of anti–MuV-HN Abs (8, 26, 27) are located around α-helices A (positions 264–269), B (positions 331–336), and C (positions 354–365) of the MuV-HN head domain (Fig. S7). Helices A, B, and C correspond to α1, α3, and α4, respectively, in the Newcastle disease virus HN protein (14). Interestingly, the similarly positioned α-helix is known as the hemagglutinin noose epitope (HNE; residues at positions 379–410) in measles virus H (28). Given that these epitopes on α-helices (helices A, B, and C on MuV-NH and HNE on measles virus H) apparently are not involved in receptor binding (15, 29), Abs against them are likely to neutralize the viruses by mechanisms other than the inhibition of receptor binding. Whereas amino acid residues in the HNE region of measles virus H are highly conserved (28), those of the MuV-HN α-helices exhibit diversity among the different genotypes of MuV (Fig. S7, *Right*). Although MuV has been considered serologically monotypic (1, 7), genotype-specific neutralizing Abs against MuV-HN can be produced at polyclonal levels (8, 9). Thus, the amino acid variability in the neutralizing epitopes may be an explanation, along with waning immunity, for the recent reports of MuV infection and reinfection among vaccinated and naturally infected populations, respectively (5, 6).

Materials and Methods

HEK293, IMR-32, and Vero cells were maintained in DMEM (Wako) supplemented with 10% (vol/vol) FBS (Sigma-Aldrich) and penicillin/streptomycin (Gibco). NCI-H358 cells were maintained in RPMI medium (Wako) supplemented with 10% (vol/vol) FBS and penicillin/streptomycin. The expression, purification, crystallization, and structure determination of proteins were carried out as described previously (15, 29), with some modifications. The MD simulation was performed with Gromacs 5.0.5 (30). The free energy values were calculated with the g_bar module of Gromacs. ITC experiments were performed using a MicroCal Auto-iTC200 calorimeter (Malvern Instruments). Binding constants were obtained by fitting the plots with a 1:1 binding model using Origin 7 (OriginLab). More detailed information is provided in *SI Materials and Methods*.

ACKNOWLEDGMENTS. We thank the beamline staff of Photon Factory (Tsukuba, Japan) for technical help during data collection, M. Tsurudome (Mie University) for the plasmids of PIV5 and PIV2, and T. Sakaguchi (Hiroshima University) for the plasmid of SeV. This study was supported by the Ministry of Education, Culture, Sports, Science, and Technology in Japan [Kakenhi Grants 26713018 (to T.H.) and 24115005 (to Y.Y.)], the Japan Society for the Promotion of Science [Postdoctoral Fellowship DC2 (to M.K. and R.M.)], the Uehara Memorial Foundation (T.H.), the Japan Foundation for Pediatric Research (T.H.), and the Takeda Science Foundation (T.H.). This study was partially supported by the Research Program on Emerging and Reemerging Infectious Diseases and the Platform Project for Supporting in Drug Discovery and Life Science Research (Platform for Drug Discovery, Informatics and Structural Life Science) from the Japan Agency for Medical Research and Development.

1. Rubin SA, Sauder CJ, Carbone KM (2013) Mumps virus. *Fields Virology*, eds Knipe DM, et al. (Lippincott Williams & Wilkins, Philadelphia), 6th Ed, Vol I, pp 1024–1041.
2. Griffin DE (2013) Measles virus. *Fields Virology*, eds Knipe DM, et al. (Lippincott Williams & Wilkins, Philadelphia), 6th Ed, Vol I, pp 1042–1069.
3. Cong H, Jiang Y, Tien P (2011) Identification of the myelin oligodendrocyte glycoprotein as a cellular receptor for rubella virus. *J Virol* 85(21):11038–11047.
4. DuBois RM, et al. (2013) Functional and evolutionary insight from the crystal structure of rubella virus protein E1. *Nature* 493(7433):552–556.
5. Latner DR, Hickman CJ (2015) Remembering mumps. *PLoS Pathog* 11(5):e1004791.
6. Yoshida N, et al. (2008) Mumps virus reinfection is not a rare event confirmed by reverse transcription loop-mediated isothermal amplification. *J Med Virol* 80(3): 517–523.
7. Rubin SA, et al. (2012) Recent mumps outbreaks in vaccinated populations: No evidence of immune escape. *J Virol* 86(1):615–620.
8. Örvell C, Alsheikhly AR, Kalantari M, Johansson B (1997) Characterization of genotype-specific epitopes of the HN protein of mumps virus. *J Gen Virol* 78(Pt 12): 3187–3193.
9. Rydbeck R, Löve A, Örvell C, Norrby E (1986) Antigenic variation of envelope and internal proteins of mumps virus strains detected with monoclonal antibodies. *J Gen Virol* 67(Pt 2):281–287.
10. Lamb RA, Parks GD (2013) Paramyxoviridae. *Fields Virology*, eds Knipe DM, et al. (Lippincott Williams & Wilkins, Philadelphia), 6th Ed, Vol I, pp 957–995.
11. Wright PF, Neumann G, Kawaoka Y (2013) Orthomyxoviruses. *Fields Virology*, eds Knipe DM, et al. (Lippincott Williams & Wilkins, Philadelphia), 6th Ed, Vol I, pp 1186–1243.
12. Reeves PJ, Callewaert N, Contreras R, Khorana HG (2002) Structure and function in rhodopsin: High-level expression of rhodopsin with restricted and homogeneous N-glycosylation by a tetracycline-inducible N-acetylglucosaminyltransferase I-negative HEK293S stable mammalian cell line. *Proc Natl Acad Sci USA* 99(21):13419–13424.
13. Walter TS, et al. (2006) Lysine methylation as a routine rescue strategy for protein crystallization. *Structure* 14(11):1617–1622.
14. Crennell S, Takimoto T, Portner A, Taylor G (2000) Crystal structure of the multifunctional paramyxovirus hemagglutinin-neuraminidase. *Nat Struct Biol* 7(11): 1068–1074.
15. Hashiguchi T, et al. (2007) Crystal structure of measles virus hemagglutinin provides insight into effective vaccines. *Proc Natl Acad Sci USA* 104(49):19535–19540.
16. Yuan P, et al. (2005) Structural studies of the parainfluenza virus 5 hemagglutinin-neuraminidase tetramer in complex with its receptor, sialyllactose. *Structure* 13(5): 803–815.
17. Lawrence MC, et al. (2004) Structure of the haemagglutinin-neuraminidase from human parainfluenza virus type III. *J Mol Biol* 335(5):1343–1357.
18. Colman PM, Hoyne PA, Lawrence MC (1993) Sequence and structure alignment of paramyxovirus hemagglutinin-neuraminidase with influenza virus neuraminidase. *J Virol* 67(6):2972–2980.
19. Nakakita S, Hirabayashi J (2016) Preparation of glycan arrays using pyridylaminated glycans. *Methods Mol Biol* 1368:225–235.
20. Imamura T, et al. (2014) Antigenic and receptor binding properties of enterovirus 68. *J Virol* 88(5):2374–2384.
21. Walther T, et al. (2013) Glycomic analysis of human respiratory tract tissues and correlation with influenza virus infection. *PLoS Pathog* 9(3):e1003223.
22. Tateno H, et al. (2008) Glycoconjugate microarray based on an evanescent-field fluorescence-assisted detection principle for investigation of glycan-binding proteins. *Glycobiology* 18(10):789–798.
23. Inou Y, et al. (2004) Molecular epidemiology of mumps virus in Japan and proposal of two new genotypes. *J Med Virol* 73(1):97–104.
24. Totani K, et al. (2003) Chemoenzymatic synthesis and application of glycopolymers containing multivalent sialyloligosaccharides with a poly(L-glutamic acid) backbone for inhibition of infection by influenza viruses. *Glycobiology* 13(5):315–326.
25. Varki A, et al. (2009) *Essentials of Glycobiology* (Cold Spring Harbor, New York), 2nd Ed.
26. Kövamees J, Rydbeck R, Orvell C, Norrby E (1990) Hemagglutinin-neuraminidase (HN) amino acid alterations in neutralization escape mutants of Kilham mumps virus. *Virus Res* 17(2):119–129.
27. Cusi MG, et al. (2001) Localization of a new neutralizing epitope on the mumps virus hemagglutinin-neuraminidase protein. *Virus Res* 74(1-2):133–137.
28. Ziegler D, et al. (1996) Protection against measles virus encephalitis by monoclonal antibodies binding to a cystine loop domain of the H protein mimicked by peptides which are not recognized by maternal antibodies. *J Gen Virol* 77(Pt 10):2479–2489.
29. Hashiguchi T, et al. (2011) Structure of the measles virus hemagglutinin bound to its cellular receptor SLAM. *Nat Struct Mol Biol* 18(2):135–141.
30. Hess B, Kutzner C, van der Spoel D, Lindahl E (2008) GROMACS 4: Algorithms for highly efficient, load-balanced, and scalable molecular simulation. *J Chem Theory Comput* 4(3):435–447.
31. Ninomiya K, et al. (2009) Amino acid substitution at position 464 in the haemagglutinin-neuraminidase protein of a mumps virus Urabe strain enhanced the virus growth in neuroblastoma SH-SY5Y cells. *Vaccine* 27(44):6160–6165.
32. Rawling J, García-Barreno B, Melero JA (2008) Insertion of the two cleavage sites of the respiratory syncytial virus fusion protein in Sendai virus fusion protein leads to enhanced cell-cell fusion and a decreased dependency on the HN attachment protein for activity. *J Virol* 82(12):5986–5998.
33. Kabsch W (2010) XDS. *Acta Crystallogr D Biol Crystallogr* 66(Pt 2):125–132.
34. McCoy AJ, et al. (2007) Phaser crystallographic software. *J Appl Cryst* 40(Pt 4):658–674.
35. Adams PD, et al. (2010) PHENIX: A comprehensive Python-based system for macromolecular structure solution. *Acta Crystallogr D Biol Crystallogr* 66(Pt 2):213–221.
36. Emsley P, Cowtan K (2004) Coot: Model-building tools for molecular graphics. *Acta Crystallogr D Biol Crystallogr* 60(Pt 12 Pt 1):2126–2132.
37. Case DA, et al. (2012) *AMBER 12 Reference Manual* (University of California San Francisco, San Francisco).
38. Kirschner KN, et al. (2008) GLYCAM06: A generalizable biomolecular force field. Carbohydrates. *J Comput Chem* 29(4):622–655.
39. Bennett CH (1976) Efficient estimation of free energy differences from Monte Carlo data. *J Comput Phys* 22(2):245–268.
40. Bussi G, Donadio D, Parrinello M (2007) Canonical sampling through velocity rescaling. *J Chem Phys* 126(1):014101.
41. Berendsen HJC, Postma JPM, van Gunsteren WF, DiNola A, Haak JR (1984) Molecular dynamics with coupling to an external bath. *J Chem Phys* 81(8):3684–3690.
42. Hess B (2008) P-LINCS: A parallel linear constraint solver for molecular simulation. *J Chem Theory Comput* 4(1):116–122.
43. Essmann U, et al. (1995) A smooth particle mesh Ewald method. *J Chem Phys* 103(19): 8577–8593.
44. Yamada A, Takeuchi K, Hishiyama M (1988) Intracellular processing of mumps virus glycoproteins. *Virology* 165(1):268–273.